PNAS RESEARCH ARTICLE | EARTH, ATMOSPHERIC, AND PLANETARY SCIENCES
ECOLOGY

Mid-Devonian ocean oxygenation enabled the expansion of animals into deeper-water habitats

Kunmanee Bubphamanee[a,b,1], Michael A. Kipp[b,c,d,1], Jana Meixnerová[a], Eva E. Stüeken[b,e], Linda C. Ivany[f], Alexander J. Bartholomew[g], Thomas J. Algeo[h,i,j], Jochen J. Brocks[k], Tais W. Dahl[l], Jordan Kinsley[k,m], François L. H. Tissot[c], and Roger Buick[a,b]

Affiliations are included on p. 6.

Edited by Lee Kump, The Pennsylvania State University, University Park, PA; received January 24, 2025; accepted July 10, 2025

The oxygenation history of Earth's surface environments has had a profound influence on the ecology and evolution of metazoan life. It was traditionally thought that the Neoproterozoic Oxygenation Event enabled the origin of animals in marine environments, followed by their persistence in aerobic marine habitats ever since. However, recent studies of redox proxies (e.g., Fe, Mo, Ce, I) have suggested that low dissolved oxygen levels persisted in the deep ocean until the Late Devonian, when the first heavily wooded ligniophyte forests raised atmospheric O_2 to modern levels. Here, we present a Paleozoic redox proxy record based on selenium enrichments and isotope ratios in fine-grained siliciclastic sediments. Our data reveal transient oxygenation of bottom waters around the Ediacaran–Cambrian boundary, followed by predominantly anoxic deep-water conditions through the Early Devonian (419 to 393 Ma). In the Middle Devonian (393 to 382 Ma), our data document the onset of permanent deep-ocean oxygenation, coincident with the spread of woody biomass across terrestrial landscapes. This episode is concurrent with the ecological occupation and evolutionary radiation of large active invertebrate and vertebrate organisms in deeper oceanic infaunal and epifaunal habitats, suggesting that the burial of recalcitrant wood from the first forests sequestered organic carbon, increased deep marine oxygen levels, and was ultimately responsible for the "mid-Paleozoic marine revolution."

paleoredox | gnathostomes | vascular plants | mid-Paleozoic marine revolution

Significance

The timing of permanent deep-ocean oxygenation is controversial; early work placed it in the Ediacaran, whereas more recent studies point to the mid-Paleozoic. Establishing the timing of this transition has profound implications for the ecological radiation and evolutionary diversification of metazoan life. Here, we better constrain the Paleozoic history of deep-ocean oxygenation using selenium geochemistry. We do not observe permanent deep-ocean oxygenation until the Middle Devonian (393 to 382 Ma), which overlaps with the "mid-Paleozoic marine revolution" in animal life. Ocean oxygenation thus provides a plausible explanation for the evolutionary changes that are documented in this interval. This rise of oxygen was likely driven by organic carbon burial during the spread of woody vascular plants across landmasses.

The role of environmental oxygen levels in shaping animal evolution has been studied for decades (1, 2). It is well accepted that the evolution of Earth from an anoxic to oxygenated state permitted the origin of aerobically respiring animal life (3). Although the sudden appearance of metazoan fossils in Ediacaran successions was once thought to derive from the permanent transition from an anoxic to a fully oxygenated ocean (4, 5), closer scrutiny of paleoredox records suggests that only limited ocean oxygenation occurred in the Ediacaran against a backdrop of predominantly anoxic conditions (6–9), with permanent deep-ocean oxygenation perhaps delayed to as late as the Devonian (10, 11). This has led to the development of more nuanced models of secular ocean oxygenation—in which shallow-marine settings may have been oxic well before ventilation of the deep ocean—with corresponding revisions to our picture of early animal evolution (12–15).

Beyond influencing the timing of their initial appearance in the fossil record, oxygen levels continued to affect animal evolution and ecology through the Phanerozoic. Marine oxygen gradients today exert strong spatial control on faunal diversity and composition. In the fossil record, the impact of oxygen on animals is apparent during hyperthermal-driven mass extinction events, when oxygen stress contributes to the extirpation or extinction of many marine animal clades (16–18). However, aside from the acknowledged constraints on the timing of the appearance of complex life, the role of oxygen as a direct driver of subsequent animal radiations is not as clear. Given that oxygen is required for large body plans in active organisms (19), its availability may have influenced the patterns of radiation of such animals and their spread into new habitats. The record of early gnathostomes (jawed vertebrates) in particular might offer an example of this. Sallan et al. (20) showed that early gnathostomes originated in shallow marine environments during the Ordovician and expanded into a variety of nearshore settings long before their appearance in deeper, outer continental shelf habitats in the Devonian. The emerging view of a predominantly anoxic deep ocean until the Devonian would be consistent with a redox-imposed habitat restriction on early vertebrates, stifling colonization of deeper-water habitats until sufficient oxygen levels were attained and stabilized. Existing paleoredox proxy records allow a broad window for deep-ocean oxygenation between the Silurian and Middle Devonian (444 to 382 Ma), yet leave uncertainty within this 60-My window. These proxy records thus

Author contributions: K.B., M.A.K., E.E.S., and R.B. designed research; K.B., M.A.K., J.M., E.E.S., L.C.I., A.J.B., T.J.A., J.J.B., T.W.D., J.K., F.L.H.T., and R.B. performed research; K.B., M.A.K., J.M., and E.E.S. analyzed data; M.K., E.E.S., and R.B. sample acquisition, project management; L.C.I., A.J.B., T.J.A., J.J.B., T.W.D., and J.K. sample acquisition; F.L.H.T. project management; and K.B., M.A.K., E.E.S., L.C.I., A.J.B., T.J.A., J.J.B., T.W.D., J.K., F.L.H.T., and R.B. wrote the paper.

The authors declare no competing interest.

This article is a PNAS Direct Submission.

[1]To whom correspondence may be addressed. Email: kubu7847@uw.edu or michael.kipp@duke.edu.

This article contains supporting information online at https://www.pnas.org/lookup/suppl/doi:10.1073/pnas.2501342122/-/DCSupplemental.

Published August 25, 2025.

provide neither sufficient temporal resolution nor redox sensitivity (i.e., high Eh) to adequately test this hypothesis.

Here, we present a redox proxy record, based on the abundance and isotopic composition of the element selenium (Se) in fine-grained siliciclastic marine sedimentary rocks, to clarify the secular oxygenation of deeper water environments, namely those comprising outer shelf to upper slope regions of continental margins. We find that, although transient pulses of deeper-water oxygenation occurred around the Ediacaran–Cambrian transition, sustained deep-ocean oxygenation is not observed until ~390 Ma, in the Middle Devonian. A gap in our record from 420 to 394 Ma—also observed in global compilations of shales and mudstones (*SI Appendix*, Fig. S1)—leaves open the possibility of an Early Devonian onset of deeper-water oxygenation. Importantly, in either case, our data document a redox transition that is roughly coincident with the appearance of gnathostomes in deeper benthic assemblages and the "mid-Paleozoic marine revolution" (21) in marine invertebrate evolution and ecology. The temporal correlation between the oxygenation of deeper habitats and these macroevolutionary phenomena suggest deep-ocean anoxia likely restricted available habitats for marine macrofauna in the earlier Paleozoic. This restriction was alleviated in the Early-Middle Devonian when the evolution of vascular land plants, woody biomass, and ultimately forests drove enhanced organic carbon burial, a rise of atmospheric O_2, and oxygenation of the ocean depths.

The Selenium Isotope Redox Proxy. Selenium isotope ratios are a well-suited proxy for tracking deep-ocean oxygenation in the ancient ocean (22). Selenium has six stable isotopes (masses 82, 80, 78, 77, 76, and 74; here, we refer to variations in the $^{82}Se/^{78}Se$ ratio in delta notation as $\delta^{82}Se$; see *Methods*) and can exist in four oxidation states (–II, 0, +IV, and +VI) in Earth's surface environments. Redox transformations of Se result in large isotopic fractionations (23) (Fig. 1*A*) and occur at relatively high redox potential (Eh) compared to many other redox proxies (Fig. 1*B*). In particular, the most significant Se isotopic fractionation occurs upon partial (nonquantitative) reduction, usually microbial, of oxidized Se species. In modern environments, nonquantitative respiration of Se oxyanions is observed at micromolar dissolved oxygen levels or higher (24), similar to thresholds for animal survival (25), making Se a useful proxy for tracking oxygen levels relevant to animal respiration.

Selenium is delivered to the ocean predominantly by rivers as dissolved Se oxyanions (SeO_4^{2-}, SeO_3^{2-}, $HSeO_3^-$) (27). This riverine input flux is thought to have an isotopic composition similar to that of the continental crust due to limited isotopic fractionation (<0.5‰) during weathering and transport (23). In seawater, Se oxyanions are taken up by marine organisms in the photic zone, with a small isotopic fractionation (<0.6‰) during assimilation (28, 29). A small amount of this organic-bound Se is exported to sediments, with the rest being regenerated as Se oxyanions (predominantly SeO_3^{2-}) during organic matter remineralization, which is not associated with Se isotopic fractionation. This water column Se oxyanion reservoir can supply Se to sediments via either adsorption to FeMn oxides (in oxic settings), which removes lighter Se isotopes ($\Delta_{seawater\text{-}adsorbed}$ ~ –1‰) (30, 31), or via reduction to Se(0) nanoparticles (in suboxic or anoxic settings), which is often followed by further reduction to Se(–II) in sediments (32). If reaction yields are nonquantitative, Se reduction can be associated with large ($\Delta_{seawater\text{-}reduced}$ up to –12‰) isotopic fractionation that favors the lighter isotopes (23, 33).

The Se isotopic composition of bulk marine sediments is a weighted mean of the various Se pools (namely organic Se, reduced Se^0 or Se^{-II}, and adsorbed Se). In settings with anoxic bottom waters, where Se oxyanion reduction goes to completion and adsorption is negligible, sediments tend to record the isotopic composition of overlying seawater (34). In settings where a stable pool of Se oxyanions persists in bottom waters, i.e., under oxic or suboxic conditions, Se adsorption to FeMn-oxides and/or nonquantitative oxyanion reduction can result in sediments with isotopic compositions lighter than seawater (34). The total concentration of Se in marine sediments is a function of both scavenging rate and marine reservoir size; reducing (both suboxic and anoxic) sediments tend to bury Se efficiently, but the maximum Se enrichment attained is a function of the Se content of deep waters. With an oxic, deep-ocean reservoir of Se oxyanions, maximum attainable Se enrichments would be higher than when the deep ocean is predominantly anoxic.

Here, we use Se abundance and isotopic composition in shales deposited in offshore settings to provide snapshots of local-to-regional redox conditions through the Paleozoic. We use a simplified scheme for interpreting $\delta^{82}Se$ values, separating samples into two groups: 1) those with crustal values, i.e., between –0.3 to +0.6‰ (35, 36), or supercrustal values above +0.6‰, and 2) those with subcrustal values with $\delta^{82}Se$ below –0.3‰. The first group likely reflects anoxic deep-water conditions, whether ferruginous or euxinic, under which Se is immobilized via reduction, as its redox transformation does not require free H_2S. Crustal $\delta^{82}Se$ values in deeper-water sediments are likely to be observed when Se oxyanions are completely reduced in anoxic bottom waters, whereas supercrustal values may derive from distillation of the Se oxyanion reservoir by incomplete reduction in nearshore suboxic zones and subsequent sequestering of residual heavy Se isotopes offshore (37). The subcrustal group likely reflects deposition in sites with a persistent deep water Se oxyanion reservoir, i.e., implying oxic to suboxic conditions locally and

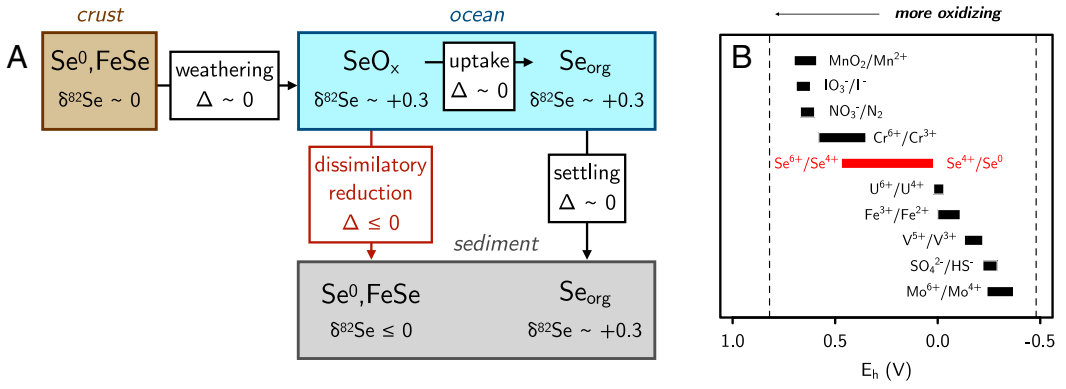

Fig. 1. A schematic of modern Se isotope mass balance (*A*), Redox potential of valence state changes in common paleo-redox proxies (*B*). Isotopic fractionations from ref. 22. Dashed lines indicate water stability field. All data collated for pH range of 7 to 8. Adapted from Kipp et al. (26).

oxygenated deep waters regionally or globally (which serve as a reservoir of Se oxyanions). Thus, the onset and persistence of subcrustal Se isotope values in offshore marine sediments over time should reflect deeper-ocean oxygenation. We note that due to the strong biological cycling and intermediate marine residence time of Se [1 to 10 kyr; ref. 27, only slightly longer than the 1 to 2 kyr ocean mixing time (38)], Se is not globally homogenized in seawater—vertical and lateral gradients in Se abundance and isotopic composition are expected in the ocean (29). Thus, Se abundance and isotopic composition in any given depositional environment provide an assessment of not global, but rather local-to-regional redox conditions: regional in the sense of recording the presence/absence of connection to a large pool of Se oxyanions (which would require a large volume of oxic bottom water); local in the sense of recording quantitative vs. partial Se oxyanion reduction in porewaters (the latter suggesting locally oxic-to-suboxic conditions). In summary, selenium isotopes provide a valuable proxy for tracking redox changes at a local to regional scale.

In contrast, highly localized proxies such as the degree of pyritization and Fe speciation reflect water column conditions in reducing environments, while the Mo isotope system serves as a well-established proxy for the global balance of oxic vs. sulfidic bottom waters. A key strength of the Se isotope system lies in its redox sensitivity at higher Eh than many existing proxies (Fig. 1*B*), making it useful to track oxygenation relevant to the threshold of animal respiration. Bulk δ^{82}Se values primarily reflect redox transformations of Se oxyanions when Se is abundant in the water column. However, its intermediate residence time and reliance on a steady supply of Se oxyanions from the global ocean present a weakness, particularly in restricted basins. In such settings, limited input of Se oxyanions can lead to quantitative reduction, leaving such settings more sensitive to local factors such as sea-level-driven primary productivity (39) and spatial heterogeneity (26). To overcome these limitations, we have compiled a large dataset of globally distributed samples in regional basins—each connected to the global ocean—that is well suited to constructing a picture of global deep-ocean oxygenation. Rather than each site providing snapshots of global trends, each interval in this compilation presents a distribution of environments and Se isotope ratios that can be used to assemble a statistical representation of deep-ocean redox.

This study aims to improve the secular record of deeper marine redox conditions throughout the Paleozoic (541 to 252 Ma), with a particular focus on the proposed broad window of oxygenation between the Silurian and Middle Devonian (444 to 382 Ma). We analyzed Se abundance and isotope ratios in 97 organic-rich mudrocks and shales spanning 31 lithological units on five continents. These were deposited in low-energy, deeper marine settings, mostly pro-delta argillites from epicontinental basins and shales from the outer shelf or upper slope regions on continental margins, roughly matching the deepest "benthic assemblage zones" in ref. 20 (paleodepth information is provided in *SI Appendix*, Table S1). We note that some samples from epicontinental seaways likely represent more restricted basins than others in the compilation, an inevitable limitation of the deep-time sedimentary record (40). However, geochemical evidence from several of these settings shows sustained connection to the open ocean (*SI Appendix*, Table S1), and we aimed to overcome this limitation by amassing a large dataset that also spans continental margin settings (*SI Appendix*). We further combined these data with 158 published Se isotope data (22) from Paleozoic mudrocks and shales from 19 additional units, giving a total Paleozoic dataset (n = 255) that exceeds published Se isotope data from the Mesozoic and Cenozoic (n = 192). All new and compiled data are provided in the *SI Appendix*.

Results

The δ^{82}Se values of all Paleozoic samples (n = 255) range from –3.3‰ to +3.8‰, with a mean (–0.10‰) that is similar to the bulk silicate Earth average value (–0.02 ± 0.05‰) estimated from mantle peridotites (36). Most shales deposited in the Paleozoic have a δ^{82}Se value within the range (–0.3 to +0.6‰) observed for crustal igneous rock samples (35). We note an interval of the most negative values (down to –3.3‰) around the Ediacaran–Cambrian transition (Fig. 2). The data return to crustal values by the Late Cambrian and gradually increase to supercrustal (~+2‰) values toward the Early Devonian. Notably, markedly negative δ^{82}Se values are persistently observed after the Middle Devonian.

Discussion

Here, we consider the Paleozoic shale Se isotope record in the context of Se isotope mass balance and other coeval paleoredox proxy records. We infer two episodes of deeper-ocean oxygenation in the Paleozoic: the first around the Ediacaran–Cambrian boundary, which was a transient event, and the second episode in the Early to Middle Devonian, which we conclude was the onset of permanent oxygenation of ocean depths.

Transient Oxygenation of Deeper Waters in the Ediacaran and Cambrian. It was once influentially suggested on the basis of Fe speciation analysis that the deep ocean became oxic after the Gaskiers glaciation (~580 Ma), thus giving rise to the Ediacaran biota and subsequent animal life (4, 5). Carbonate δ^{13}C records, particularly the Shuram excursion, were also interpreted as to reflect deep-ocean oxygenation with concomitant oxidation of a dissolved organic carbon reservoir (44). However, subsequent work challenged both the Fe speciation (11) and δ^{13}C (45, 46) interpretations, instead invoking only transient oxygenation during the Ediacaran. This has also been borne out in more recent studies using other paleoredox proxies (e.g., refs. 6–9).

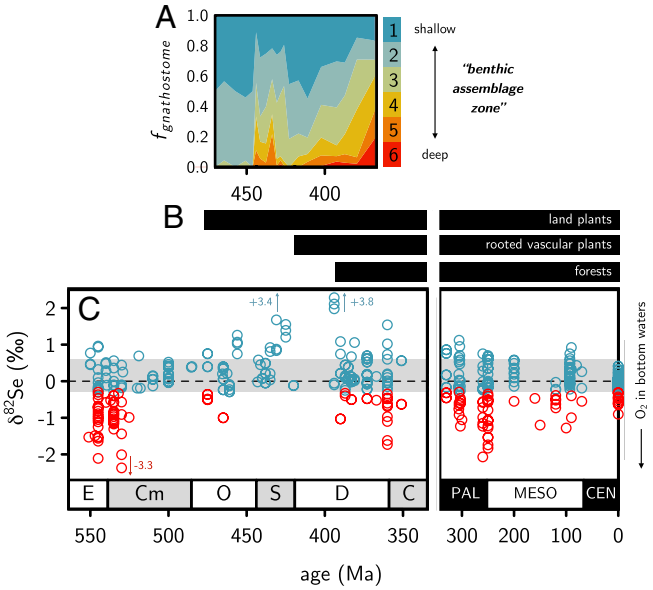

Fig. 2. Habitat distribution of mid-Paleozoic gnathostomes (*A*), evolution of terrestrial ecosystems (*B*), and secular record of Se isotope ratios in marine sedimentary rocks (*C*). Relative occurrence rates ($f_{gnathostome}$) of fossil gnathostomes in benthic assemblage zones were compiled by Sallan et al. (20), where BA1 to BA6 denote shallow to deep marine habitats (41). Record of terrestrial ecosystem evolution from refs. 42 and 43. In panel *C*, the dashed line denotes crustal average, with uncertainty range in gray shading. Blue circles denote crustal or supercrustal Se isotope ratios; red circles denote subcrustal values. Note change in *x*-axis scale at ca. 340 Ma.

Our data are consistent with the later, more nuanced view of transient oxygenation in the Ediacaran and Early Cambrian. Multiple localities record strongly negative δ^{82}Se values around the Ediacaran–Cambrian boundary (47, 48), consistent with nonquantitative reduction of a large Se oxyanion reservoir. In the same interval, Se abundance in shales reaches ~100 ppm (49), Mo isotopes in euxinic black shales approach modern values (+2.3‰) (50), and negative Ce anomalies are observed in carbonates (51) (Fig. 3). These records collectively support at least episodic seafloor oxygenation. However, shales return to crustal δ^{82}Se values later in the Cambrian. Similar trends toward more reducing conditions are observed in other geochemical proxies: shale Se enrichments decrease by an order of magnitude, black shale Mo isotope ratios drop toward the riverine input value, and Ce anomalies become less pronounced (Fig. 3). These patterns reinforce the inference that seafloor oxygenation around the Ediacaran–Cambrian boundary was only temporary.

Between ~530 and ~420 Ma, shale δ^{82}Se predominantly falls within the crustal range, despite some supercrustal values, whereas subcrustal results nearly disappear. This indicates a shift back to anoxic bottom waters without access to a large deep-ocean Se oxyanion reservoir. The sporadic appearance of subcrustal δ^{82}Se values in the Ordovician likely reflects transient oxygenation events driven by increased availability of Se oxyanions at regional scales. The increase in prevalence of supercrustal δ^{82}Se values between 475 and 420 Ma could indicate enhanced isotopic distillation in restricted basins; such effects have been observed in later Paleozoic epeiric seas (26) and are thought to be driven by partial Se oxyanion reduction in shallower (perhaps estuarine) settings (37). Notably, our samples from this interval are dominated by epicontinental sea settings (*SI Appendix*, Table S1), coinciding with a prolonged greenhouse climate during the late Cambrian through Early Devonian, during which rising eustatic sea level flooded continental interiors. However, samples from both open-oceans and epicontinental seas exhibit similar trends of δ^{82}Se values, supporting our assessment that a large compilation of regional basins can reliably reflect broader deeper-ocean redox conditions. Importantly for our purposes, the dearth of subcrustal values in the fine-grained siliciclastic sediments studied here suggests the absence of deeper-water oxygenation.

Permanent Oxygenation of Deeper Waters in the Devonian. A clear change in all redox proxy records is observed after ~390 Ma (Figs. 2 and 3). Shale δ^{82}Se data consistently exhibit subcrustal values, suggesting nonquantitative oxyanion reduction and implying (sub-)oxic conditions down to the sediment–water interface at our sampling localities. Since we observe these signatures in multiple localities, the data likely indicate that widespread oxygenation of the deep ocean was achieved by that time (Figs. 2 and 3). Average shale Se abundance from 530 to 410 Ma is $1.1^{+4.0}_{-0.9}$ ppm (geometric mean, 1 SD) and, after a gap in the record, is $5.6^{+9.9}_{-3.6}$ ppm (geometric mean, 1 SD) from 394 to 350 Ma (Fig. 3), including many values >50 ppm, consistent with a larger marine dissolved Se reservoir in a well-oxygenated ocean. Euxinic black shale Mo isotope data likewise shift toward the modern seawater value by 390 Ma, though we acknowledge a lack of data in the Silurian and Early Devonian (443 to 393 Ma) (Fig. 3). Finally, a strong negative Ce anomaly around ~380 Ma reflects vigorous Ce(IV) removal from a well-oxygenated water column (Fig. 3). Thus, our findings constrain the timing of sustained deeper-ocean oxygenation to have occurred by ~390 Ma (Middle Devonian), though perhaps starting in the prior interval during which data are scarce (419 to 390 Ma; Early Devonian). We also note that COPSE—a mechanistic forward biogeochemical model of carbon, oxygen and nutrient cycles that does not use the redox proxy data above as inputs (53)—predicts that the seafloor experienced stepwise oxygenation, with a first pulse from 450 to 390 Ma and a large swing toward fully oxygenated conditions after ~390 Ma, broadly consistent with our Se record and the other compiled redox proxy data (Fig. 3).

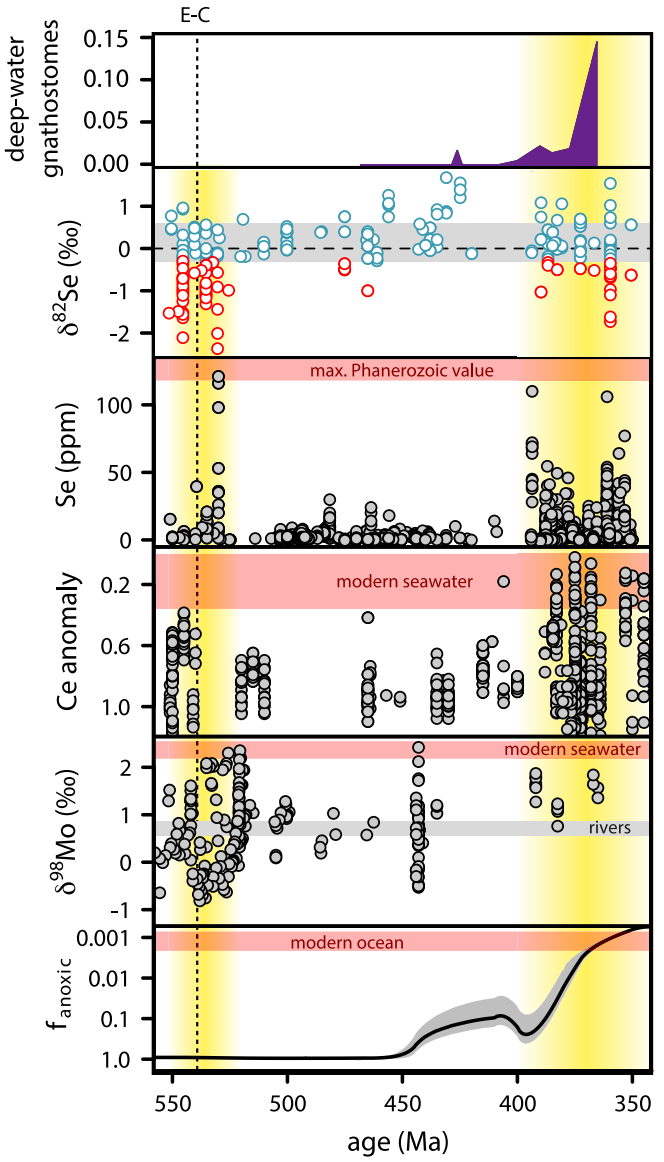

Fig. 3. Records of vertebrate fossil distribution, marine redox proxies, and modeled ocean anoxia through the early-mid Paleozoic. Two proposed ocean oxygenation intervals are highlighted in yellow. Both intervals feature not only subcrustal Se isotope ratios in shales, but also large shale Se enrichments (49), high black shale Mo isotope ratios (50), and negative Ce anomalies (52). We infer that the first interval near the Ediacaran–Cambrian boundary did not result in permanent deep-ocean oxygenation, whereas after 390 Ma, the deep ocean experienced sustained oxygenation, consistent with the COPSE model (53) that invokes a rise of O_2 at that time due to terrestrial biomass burial. It is only after this Devonian oxygenation that vertebrates consistently appear in the deepest benthic assemblage zone (*Top* panel shows the relative occurrence of gnathostomes in BA6, as in Fig. 2*A*) (20). A more detailed description of compiled proxies and models can be found in the *Methods*. E-C = Ediacaran–Cambrian boundary. Modern or Phanerozoic maximum proxy values shown in red shading. All axes, except Se isotope data, are oriented such that more oxygenated conditions plot upward.

Evolutionary Causes and Consequences of Devonian Ocean Oxygenation. Selenium abundance and isotope values offer valuable insights into deeper-ocean oxygenation and oxygen availability in marine systems. We propose that Se isotope

data provide a direct record of two episodes of deeper-ocean oxygenation during the latest Precambrian and early Paleozoic. The first of these oxygenation events was transient, occurring in the Ediacaran and earliest Cambrian. This event has been well-documented by numerous geochemical proxies and coincides with the first appearance of benthic animals, supporting an important role of oxygen in the origins of animal life (12–15). The drivers of this first ocean oxygenation remain unresolved, with proposed mechanisms including post-Marinoan environmental change (54, 55) and increased bioturbation (56), both potentially disrupting phosphorus cycling and enhancing organic carbon burial, thereby facilitating marine oxygen accumulation. Alternative mechanisms, such as physical processes and biological innovations, have been proposed and are reviewed elsewhere. The second episode of marine oxygenation happened in the Early to Middle Devonian, between 420 and 390 Ma, and unlike the first, this reflects a lasting shift toward a fully oxygenated ocean.

Although these data do not specifically constrain the cause of Devonian oxygenation, a prior connection has previously been drawn to enhanced organic carbon burial during the spread of woody vascular plants on land (57, 58). Vascular plants emerged in the Silurian (444 to 419 Ma) and diversified into the Early Devonian (419 to 393 Ma) when woody tissue evolved during the Emsian (~400 Ma) (59, 60), with the first forests appearing ~390 Ma (61) (Fig. 2). Land plants, and particularly woody biomass composed of phosphorus-poor biopolymers, have much higher molar C/P ratios than marine organic matter (10, 50, 62, 63). The expansion of land plants enhanced continental weathering, increased phosphorus input into the ocean, and stimulated primary productivity. Together, terrestrial and marine productivity would cause a global increase in organic carbon burial and thus leave surplus O_2 in the atmosphere (57, 63, 64). As noted above, our redox proxy record compilation suggests that persistent deeper-ocean oxygenation occurred at or shortly before 390 Ma, coincident with the Middle Devonian rise of forests (42, 65). With the latest COPSE model suggesting atmospheric O_2 began rising during the Silurian, proceeding global Devonian ocean oxygenation (66), we cannot rule out an Early Devonian (419 to 393 Ma) onset of deep-ocean oxygenation due to our lack of Se isotope data in this interval. However, other redox proxies and the COPSE model all point to the major marine redox transition occurring in the Middle Devonian (Fig. 3). Taken together, these records support a causal link between woody biomass burial, the rise of atmospheric O_2, and oxygenation of ocean depths.

Beyond the terrestrial drivers of this transition, Middle Devonian deep-ocean oxygenation coincides with a number of marine ecosystem changes, some of which have been collectively referred to as the "mid-Paleozoic marine revolution" (21). These include an increase in the maximum body size and total metabolic activity of marine invertebrates, enhanced and deepened seafloor bioturbation, the diversification of predators and nektonic organisms, and the colonization of deeper-ocean settings by early vertebrates. The size to which animals with poor ventilation and circulation can grow is influenced by oxygen availability (19, 67), and so it is notable that there is a 1.5 log unit increase in maximum invertebrate biovolume through the Early and Middle Devonian (68), coincident with the window of ocean oxygenation (420 to 390 Ma) identified by the Se isotope record. Biovolume varies across taxa even within a single phylum (69), but it is significant that this trend is most obvious in sessile benthic groups as opposed to vagile infaunal and active swimmers. Total metabolic activity across taxa with similar architectures also varied through this interval, with more active bivalve metabolism increasing by 1 log unit, whereas sessile brachiopods decreased metabolic activity by 50% (70), again perhaps reflecting the effect of oxygen availability on organisms of differing physiology.

Higher dissolved oxygen levels also allow deeper oxygen penetration into sediment porewaters, potentially enabling deeper bioturbation. *Zoophycos*, a prominent Phanerozoic ichnofossil, first underwent a transition during the Devonian from shallow infauna before to deep-tier infauna after. This early transition began in the late Silurian, with its first appearance in the deeper bathyal realm at the Early-Middle Devonian boundary (71). In support of this argument, broader ichnological studies indicate limited sediment mixing by bioturbation until at least the Late Silurian (72, 73). Nekton largely replaced bottom-dwelling relatives during the Devonian as well, most notably in fishes but also in cephalopods. This "nekton revolution" has been linked to plankton diversification enabled by increased nutrient supply (74); however, our Se redox record suggests that higher oxygen levels within the water column instead (or in addition) may have brought about an expansion in more active swimming organisms. The mid-Paleozoic radiation of durophagous predators, again principally fish but also arthropods (21), coincided with the Middle Devonian redox transition, as does the appearance of gnathostomes in the deepest benthic assemblages (Figs. 2 and 3). We therefore suggest that delayed oxygenation of the deeper ocean may have postponed a significant radiation of jawed vertebrates and their expansion into deeper marine environments until the Middle Devonian, concurrent with significant evolutionary and ecological changes in invertebrate faunas.

Conclusions

Oxidative continental weathering, driven by atmospheric oxygen, enriches the ocean with redox-sensitive trace metals, including Se. Subcrustal Se isotope values in marine sediments indicate non-quantitative reduction of Se oxyanions, suggesting deposition in environments closely linked to a large, oxic reservoir. An interval of subcrustal δ^{82}Se values observed at the Ediacaran–Cambrian boundary signals a transient episode of deep-ocean oxygenation. However, from the Late Cambrian up to the Early Devonian (530 to 420 Ma), shale δ^{82}Se values returned to crustal values, indicating a prevalence of anoxic conditions in bottom waters up to that time. The reappearance of subcrustal Se isotope values in black shales deposited in the Middle Devonian (~390 Ma) and thereafter documents the onset of persistent deeper-ocean oxygenation. We speculate that this transition was driven by the advent of woody land plants, which increased the global rate of organic carbon burial. The onset of deeper ocean oxygenation in our proposed window between 420 to 390 Ma set the stage for the expansion of larger, more active, and more ecologically complex organisms in marine ecosystems. The return of pervasively anoxic conditions in deep marine settings after the Ediacaran–Cambrian oxygenation event may thus have hindered the diversification of deep-water jawed vertebrates for over 100 My.

Methods

Samples were prepared for isotopic analysis following published methods (75). Samples were pulverized and ~1 g homogenized powder was digested using a combination of concentrated HF, $HClO_4$, and 8 M HNO_3 for ~2 d at 130 °C. Digests were evaporated to incipient dryness and additional $HClO_4$ was added until all organic matter was visibly removed. After again evaporating to incipient dryness, 6 M HCl was added, and samples were boiled for 30 min to convert all Se to Se^{IV}. These solutions were diluted to 0.6 M HCl and passed through thiol cotton fiber (TCF) columns for Se purification. Most matrix elements were eluted in this process, and Se was then recovered from the TCF by boiling in concentrated HNO_3 for 20 min. Released Se was recovered via centrifugation

and dried to a ~0.5 mL drop, then reconstituted in aqua regia (3:1 HCl:HNO_3). This solution was dried down at <60 °C to volatilize germanium that was retained on the resin. Again upon reaching a ~0.5 mL drop, the samples were reconstituted in 6 M HCl, boiled for 30 min to convert Se to Se^{IV}, and diluted to 0.6 M HCl for analysis.

Selenium isotope ratios were analyzed using a Nu Plasma Multicollector Inductively Coupled Plasma Mass Spectrometer (MC-ICP-MS) at University of Washington and a Thermo NeptunePlus MC-ICP-MS in the Isotoparium at California Institute of Technology. Sample data were corrected using standard-sample bracketing and reported in delta notation relative to NIST SRM 3149. Isobaric interferences from argon dimers were corrected following published protocols (75, 76); other isobaric interferences were not corrected as they have negligible impact on the reported ratios compared to our external reproducibility. We report $\delta^{82/78}$Se ratios in the main text as these are the least affected by isobaric interferences in our correction scheme, but we note that all samples exhibit mass-dependent fractionation (*SI Appendix*, Fig. S2), and thus conversion between ratios is possible to compare our data to studies that report other isotopic pairs. Sample solutions were analyzed multiple times whenever possible; data are reported with 2σ (SE) uncertainty. Typical analytical precision was ±0.18‰ (2σ) based on all replicate sample analyses. Analyses of the UW-McRae in-house standard (+0.86 ± 0.06‰, 2σ, $n = 10$) and USGS SGR-1b (–0.20‰, $n = 1$) were consistent with published data (26, 34, 35, 37, 75, 77–80).

Additional selenium concentration data from marine sedimentary rocks were downloaded from the Sedimentary Geochemistry and Paleoenvironments Project (49). Published redox proxy records compiled in Fig. 3 include Mo isotopes (10, 50), Ce anomalies (51), and seafloor anoxia estimates from the COPSE model (53).

Data, Materials, and Software Availability. New data generated from this study were included in Dataset S1. Previously published data were used for this work (22, 23, 34, 37, 39, 47, 48, 77, 81–85). Our manuscript includes previously published data, plotted in Figs. 2 and 3 and all datasets were included in Dataset S2. All other data are included in the article and/or supporting information.

ACKNOWLEDGMENTS. We thank Scott Kuehner, Bruce Nelson, Fang-Zhen Teng, and Yan Hu for analytical assistance. Tom Johnson graciously provided an aliquot of NIST SRM 3149 for method set up at Caltech. L.C.I. thanks Carl Brett for years of conversation about Silurian–Devonian ecosystems. M.A.K. was supported by an NSF Graduate Research Fellowship, an Agouron Institute Postdoctoral Fellowship, and NSF grant MGG-2054892 (to F.L.H.T.). Additional support was provided by the NASA Astrobiology Institute Virtual Planetary Laboratory Grant 80NSSC19K0829.

Author affiliations: [a]Department of Earth and Space Sciences, University of Washington, Seattle, WA 98195-1310; [b]Virtual Planetary Laboratory, NASA Nexus for Exoplanet Systems Science, Seattle, WA 98195-1310; [c]The Isotoparium, Division of Geological and Planetary Sciences, California Institute of Technology, Pasadena, CA 91125; [d]Division of Earth and Climate Sciences, Nicholas School of the Environment, Duke University, Durham, NC 27708; [e]School of Earth and Environmental Sciences, University of St. Andrews, St. Andrews, Scotland KY16 9AL, United Kingdom; [f]Department of Earth and Environmental Sciences, Syracuse University, Syracuse, NY 13210; [g]Geology Department, State University of New York, New Paltz, NY 12561-2443; [h]Department of Geosciences, University of Cincinnati, Cincinnati, OH 45221-0013; [i]State Key Laboratories of Geomicrobiology and Environmental Geology Changes and Geological Processes and Mineral Resources, China University of Geosciences, Wuhan, Wuhan 430074, China; [j]State Key Laboratory of Oil and Gas Reservoir Geology and Exploitation, Chengdu University of Technology, Chengdu 610059, China; [k]Research School of Earth Sciences, Australian National University, Canberra, ACT 2601, Australia; [l]Department of Geosciences and Natural Resource Management, University of Copenhagen, Øster Voldgade 10, 1350 Copenhagen, Denmark; and [m]Chemostrat Australia Pty. Ltd, Perth, WA 6005, Australia

1. A. Krogh, The rate of diffusion of gases through animal tissues, with some remarks on the coefficient of invasion. *J. Physiol.* **52**, 391 (1919).
2. J. Nursall, Oxygen as a prerequisite to the origin of the Metazoa. *Nature* **183**, 1170–1172 (1959).
3. A. H. Knoll, *Life on a Young Planet: The First Three Billion Years of Evolution on Earth* (Princeton University Press, 2015).
4. D. E. Canfield, S. W. Poulton, G. M. Narbonne, Late-neoproterozoic deep-ocean oxygenation and the rise of animal life. *Science* **315**, 92–95 (2007).
5. Y. Shen, T. Zhang, P. F. Hoffman, On the coevolution of Ediacaran oceans and animals. *Proc. Natl. Acad. Sci. U.S.A.* **105**, 7376–7381 (2008).
6. B. Kendall *et al.*, Uranium and molybdenum isotope evidence for an episode of widespread ocean oxygenation during the late Ediacaran Period. *Geochim. Cosmochim. Acta* **156**, 173–193 (2015).
7. S. K. Sahoo *et al.*, Oceanic oxygenation events in the anoxic Ediacaran ocean. *Geobiology* **14**, 457–468 (2016).
8. R. Tostevin *et al.*, Uranium isotope evidence for an expansion of anoxia in terminal Ediacaran oceans. *Earth Planet. Sci. Lett.* **506**, 104–112 (2019).
9. C. M. Ostrander *et al.*, Thallium isotope ratios in shales from South China and northwestern Canada suggest widespread O2 accumulation in marine bottom waters was an uncommon occurrence during the Ediacaran Period. *Chem. Geol.* **557**, 119856 (2020).
10. T. W. Dahl *et al.*, Devonian rise in atmospheric oxygen correlated to the radiations of terrestrial plants and large predatory fish. *Proc. Natl. Acad. Sci. U.S.A.* **107**, 17911–17915 (2010).
11. E. A. Sperling *et al.*, Statistical analysis of iron geochemical data suggests limited late Proterozoic oxygenation. *Nature* **523**, 451–454 (2015).
12. R. Tostevin, B. J. W. Mills, Reconciling proxy records and models of Earth's oxygenation during the Neoproterozoic and Palaeozoic. *Interface Focus* **10**, 20190137 (2020).
13. D. B. Cole *et al.*, On the co-evolution of surface oxygen levels and animals. *Geobiology* **18**, 260–281 (2020).
14. E. A. Sperling *et al.*, Breathless through time: Oxygen and animals across Earth's history. *Biol. Bull.* **243**, 184–206 (2022).
15. C. M. Ostrander, Mulling and nulling the coeval rise of Ediacaran oxygen and animals. *Earth Planet. Sci. Lett.* **614**, 118187 (2023).
16. P. B. Wignall, R. J. Twitchett, Oceanic anoxia and the end Permian mass extinction. *Science* **272**, 1155–1158 (1996).
17. R. G. Stockey, A. Pohl, A. Ridgwell, S. Finnegan, E. A. Sperling, Decreasing Phanerozoic extinction intensity as a consequence of Earth surface oxygenation and metazoan ecophysiology. *Proc. Natl. Acad. Sci. U.S.A.* **118**, e2101900118 (2021).
18. J. L. Penn, C. Deutsch, J. L. Payne, E. A. Sperling, Temperature-dependent hypoxia explains biogeography and severity of end-Permian marine mass extinction. *Science* **362**, eaat1327 (2018).
19. J. L. Payne *et al.*, Two-phase increase in the maximum size of life over 3.5 billion years reflects biological innovation and environmental opportunity. *Proc. Natl. Acad. Sci. U.S.A.* **106**, 24–27 (2009).
20. L. Sallan, M. Friedman, R. S. Sansom, C. M. Bird, I. J. Sansom, The nearshore cradle of early vertebrate diversification. *Science* **362**, 460–464 (2018).
21. P. W. Signor, C. E. Brett, The mid-Paleozoic precursor to the Mesozoic marine revolution. *Paleobiology* **10**, 229–245 (1984).
22. E. E. Stüeken, M. A. Kipp, *Selenium Isotope Paleobiogeochemistry* (Cambridge University Press, 2020).
23. T. M. Johnson, A review of mass-dependent fractionation of selenium isotopes and implications for other heavy stable isotopes. *Chem. Geol.* **204**, 201–214 (2004).
24. E. L. Rue, G. J. Smith, G. A. Cutter, K. W. Bruland, The response of trace element redox couples to suboxic conditions in the water column. *Deep Sea Res. Part Oceanogr. Res. Pap.* **44**, 113–134 (1997).
25. D. B. Mills *et al.*, Oxygen requirements of the earliest animals. *Proc. Natl. Acad. Sci. U.S.A.* **111**, 4168–4172 (2014).
26. M. A. Kipp, T. J. Algeo, E. Stüeken, R. Buick, Basinal hydrographic and redox controls on selenium enrichment and isotopic fractionation in Paleozoic black shales. *Geochim. Cosmochim. Acta* **287**, 229–250 (2020).
27. E. E. Stüeken, Selenium isotopes as a biogeochemical proxy in deep time. *Rev. Mineral. Geochem.* **82**, 657–682 (2017).
28. S. K. Clark, T. M. Johnson, Selenium stable isotope investigation into selenium biogeochemical cycling in a lacustrine environment: Sweitzer Lake, Colorado. *J. Environ. Qual.* **39**, 2200–2210 (2010).
29. Y. Chang, J. Zhang, J.-Q. Qu, Y. Xue, Precise selenium isotope measurement in seawater by carbon-containing hydride generation-desolvation-MC-ICP-MS after thiol resin preconcentration. *Chem. Geol.* **471**, 65–73 (2017).
30. W. Xu *et al.*, Selenium isotope fractionation during adsorption by Fe, Mn and Al oxides. *Geochim. Cosmochim. Acta* **272**, 121–136 (2020).
31. H.-B. Qin *et al.*, Molecular-scale insight into selenium isotope fractionation caused by adsorption on Fe (oxyhydr) oxides. *Geochim. Cosmochim. Acta* **361**, 24–39 (2023).
32. D. J. Velinsky, G. A. Cutter, Determination of elemental selenium and pyrite-selenium in sediments. *Anal. Chim. Acta* **235**, 419–425 (1990).
33. K. Schilling *et al.*, Mass-dependent selenium isotopic fractionation during microbial reduction of seleno-oxyanions by phylogenetically diverse bacteria. *Geochim. Cosmochim. Acta* **276**, 274–288 (2020).
34. E. E. Stüeken *et al.*, The evolution of the global selenium cycle: Secular trends in Se isotopes and abundances. *Geochim. Cosmochim. Acta* **162**, 109–125 (2015).
35. O. Rouxel, J. Ludden, J. Carignan, L. Marin, Y. Fouquet, Natural variations of Se isotopic composition determined by hydride generation multiple collector inductively coupled plasma mass spectrometry. *Geochim. Cosmochim. Acta* **66**, 3191–3199 (2002).
36. M. I. Varas-Reus, S. König, A. Yierpan, J.-P. Lorand, R. Schoenberg, Selenium isotopes as tracers of a late volatile contribution to Earth from the outer Solar System. *Nat. Geosci.* **12**, 779–782 (2019).
37. M. A. Kipp, E. E. Stüeken, A. Bekker, R. Buick, Selenium isotopes record extensive marine suboxia during the Great Oxidation Event. *Proc. Natl. Acad. Sci. U.S.A.* **114**, 875–880 (2017).
38. W. S. Broecker, T.-H. Peng, *Tracers in the Sea* (Lamont-Doherty Geological Observatory, Columbia University, 1982).
39. A. J. T. Shore, Selenium geochemistry and isotopic composition of sediments from the Cariaco Basin and the Bermuda Rise: A comparison between a restricted basin and the open ocean over the last 500 ka. https://hdl.handle.net/2381/9010. Deposited 25 January 2011.
40. S. E. Peters, J. M. Husson, Sediment cycling on continental and oceanic crust. *Geology* **45**, 323–326 (2017).
41. A. J. Boucot, Standing diversity of fossil groups in successive intervals of geologic time viewed in the light of changing levels of provincialism. *J. Paleontol.* **49**, 1105–1111 (1975).
42. T. J. Algeo, S. E. Scheckler, Terrestrial-marine teleconnections in the Devonian: Links between the evolution of land plants, weathering processes, and marine anoxic events. *Philos. Trans. R. Soc. Lond. B. Biol. Sci.* **353**, 113–130 (1998).
43. M. P. D'Antonio, D. E. Ibarra, C. K. Boyce, Land plant evolution decreased, rather than increased, weathering rates. *Geology* **48**, 29–33 (2020).

44. D. A. Fike, J. P. Grotzinger, L. M. Pratt, R. E. Summons, Oxidation of the Ediacaran ocean. *Nature* **444**, 744–747 (2006).
45. F. A. Macdonald *et al.*, The stratigraphic relationship between the Shuram carbon isotope excursion, the oxygenation of Neoproterozoic oceans, and the first appearance of the Ediacara biota and bilaterian trace fossils in northwestern Canada. *Chem. Geol.* **362**, 250–272 (2013).
46. D. P. Schrag, J. A. Higgins, F. A. Macdonald, D. T. Johnston, Authigenic carbonate and the history of the global carbon cycle. *Science* **339**, 540–543 (2013).
47. H. Wen *et al.*, Selenium isotopes trace anoxic and ferruginous seawater conditions in the Early Cambrian. *Chem. Geol.* **390**, 164–172 (2014).
48. P. A. P. Strandmann *et al.*, Selenium isotope evidence for progressive oxidation of the Neoproterozoic biosphere. *Nat. Commun.* **6**, 10157 (2015).
49. Ú. C. Farrell *et al.*, The sedimentary geochemistry and paleoenvironments project. *Geobiology* **19**, 545–556 (2021).
50. X. Chen *et al.*, Rise to modern levels of ocean oxygenation coincided with the Cambrian radiation of animals. *Nat. Commun.* **6**, 7142 (2015).
51. M. W. Wallace, A. Shuster, A. Greig, N. J. Planavsky, C. P. Reed, Oxygenation history of the Neoproterozoic to early Phanerozoic and the rise of land plants. *Earth Planet. Sci. Lett.* **466**, 12–19 (2017).
52. J. Stacey *et al.*, Ocean oxygenation and ecological restructuring caused by the late Paleozoic evolution of land plants. *Geology* **52**, 948–952 (2024).
53. T. M. Lenton, S. J. Daines, B. J. Mills, COPSE reloaded: An improved model of biogeochemical cycling over Phanerozoic time. *Earth Sci. Rev.* **178**, 1–28 (2017).
54. G. Jiang *et al.*, Organic carbon isotope constraints on the dissolved organic carbon (DOC) reservoir at the Cryogenian–Ediacaran transition. *Earth Planet. Sci. Lett.* **299**, 159–168 (2010).
55. S. K. Sahoo *et al.*, Ocean oxygenation in the wake of the Marinoan glaciation. *Nature* **489**, 546–549 (2012).
56. R. A. Boyle *et al.*, Stabilization of the coupled oxygen and phosphorus cycles by the evolution of bioturbation. *Nat. Geosci.* **7**, 671–676 (2014).
57. T. M. Lenton *et al.*, Earliest land plants created modern levels of atmospheric oxygen. *Proc. Natl. Acad. Sci. U.S.A.* **113**, 9704–9709 (2016).
58. M. Elrick *et al.*, Major early-middle Devonian oceanic oxygenation linked to early land plant evolution detected using high-resolution U isotopes of marine limestones. *Earth Planet. Sci. Lett.* **581**, 117410 (2022).
59. P. Gerrienne *et al.*, A simple type of wood in two early Devonian plants. *Science* **333**, 837–837 (2011).
60. K. C. Pfeiler, A. M. F. Tomescu, Mosaic assembly of regulatory programs for vascular cambial growth: A view from the Early Devonian. *New Phytol.* **240**, 529–541 (2023).
61. N. S. Davies, W. J. McMahon, C. M. Berry, Earth's earliest forest: Fossilized trees and vegetation-induced sedimentary structures from the Middle Devonian (Eifelian) Hangman Sandstone Formation, Somerset and Devon, SW England. *J. Geol. Soc.* **181**, jgs2023-204 (2024).
62. T. J. Algeo, E. Ingall, Sedimentary Corg: P ratios, paleocean ventilation, and Phanerozoic atmospheric pO2. *Palaeogeogr. Palaeoclimatol. Palaeoecol.* **256**, 130–155 (2007).
63. L. R. Kump, Terrestrial feedback in atmospheric oxygen regulation by fire and phosphorus. *Nature* **335**, 152–154 (1988).
64. N. M. Bergman, COPSE: A new model of biogeochemical cycling over Phanerozoic time. *Am. J. Sci.* **304**, 397–437 (2004).
65. E. Capel *et al.*, The Silurian–Devonian terrestrial revolution: Diversity patterns and sampling bias of the vascular plant macrofossil record. *Earth Sci. Rev.* **231**, 104085 (2022).
66. T. W. Dahl *et al.*, Low atmospheric CO2 levels before the rise of forested ecosystems. *Nat. Commun.* **13**, 7616 (2022).
67. N. A. Heim *et al.*, Respiratory medium and circulatory anatomy constrain size evolution in marine macrofauna. *Paleobiology* **46**, 288–303 (2020).
68. N. A. Heim, M. L. Knope, E. K. Schaal, S. C. Wang, J. L. Payne, Cope's rule in the evolution of marine animals. *Science* **347**, 867–870 (2015).
69. D. K. Moss, L. C. Ivany, D. S. Jones, Fossil bivalves and the sclerochronological reawakening. *Paleobiology* **47**, 551–573 (2021).
70. J. L. Payne, N. A. Heim, M. L. Knope, C. R. McClain, Metabolic dominance of bivalves predates brachiopod diversity decline by more than 150 million years. *Proc. Biol. Sci.* **281**, 20133122 (2014).
71. L.-J. Zhang, R.-Y. Fan, Y.-M. Gong, Zoophycos macroevolution since 541 Ma. *Sci. Rep.* **5**, 14954 (2015).
72. L. G. Tarhan, M. L. Droser, N. J. Planavsky, D. T. Johnston, Protracted development of bioturbation through the early Palaeozoic Era. *Nat. Geosci.* **8**, 865–869 (2015).
73. L. G. Tarhan, The early Paleozoic development of bioturbation—Evolutionary and geobiological consequences. *Earth Sci. Rev.* **178**, 177–207 (2018).
74. C. Klug *et al.*, The Devonian nekton revolution. *Lethaia* **43**, 465–477 (2010).
75. E. E. Stüeken, J. Foriel, B. K. Nelson, R. Buick, D. C. Catling, Selenium isotope analysis of organic-rich shales: Advances in sample preparation and isobaric interference correction. *J. Anal. At. Spectrom.* **28**, 1734–1749 (2013).
76. M.-L. Pons, M.-A. Millet, G. N. Nowell, S. Misra, H. M. Williams, Precise measurement of selenium isotopes by HG-MC-ICPMS using a 76–78 double-spike. *J. Anal. At. Spectrom.* **35**, 320–330 (2020).
77. K. Mitchell *et al.*, Selenium as paleo-oceanographic proxy: A first assessment. *Geochim. Cosmochim. Acta* **89**, 302–317 (2012).
78. P. A. P. von Strandmann, C. D. Coath, D. C. Catling, S. W. Poulton, T. Elliott, Analysis of mass dependent and mass independent selenium isotope variability in black shales. *J. Anal. At. Spectrom.* **29**, 1648–1659 (2014).
79. T. Kurzawa, S. König, J. Labidi, A. Yierpan, R. Schoenberg, A method for Se isotope analysis of low ng-level geological samples via double spike and hydride generation MC-ICP-MS. *Chem. Geol.* **466**, 219–228 (2017).
80. M. A. Kipp, A. Lepland, R. Buick, Redox fluctuations, trace metal enrichment and phosphogenesis in the ~ 2.0 Ga Zaonega Formation. *Precambrian Res.* **343**, 105716 (2020).
81. M. A. Kipp, T. J. Algeo, E. E. Stüeken, R. Buick, Basinal hydrographic and redox controls on selenium enrichment and isotopic composition in Paleozoic black shales. *Geochim. Cosmochim. Acta* **287**, 229–250 (2020).
82. K. Mitchell, S. Z. Mansoor, P. R. D. Mason, T. M. Johnson, P. Van Cappellen, Geological evolution of the marine selenium cycle: Insights from the bulk shale δ 82/76 Se record and isotope mass balance modeling. *Earth Planet. Sci. Lett.* **441**, 178–187 (2016).
83. E. E. Stüeken, R. Buick, A. D. Anbar, Selenium isotopes support free O2 in the latest Archean. *Geology* **43**, 259–262 (2015).
84. E. E. Stüeken, J. Foriel, R. Buick, S. D. Schoepfer, Selenium isotope ratios, redox changes and biological productivity across the end-Permian mass extinction. *Chemical Geology* **410**, 28–39 (2015).
85. M. C. Koehler, R. Buick, M. A. Kipp, E. E. Stüeken, J. Zaloumis, Transient surface ocean oxygenation recorded in the ~2.66-Ga Jeerinah Formation, Australia. *Proc. Natl. Acad. Sci. U.S.A.* **115**, 7711–7716 (2018).